Transformers Can Do Bayesian Inference

Samuel Müller [1]   **Noah Hollmann** [2]   **Sebastian Pineda** [1]   **Josif Grabocka** [1]   **Frank Hutter** [1,3]
[1] University of Freiburg, [2] Charité Berlin, [3] Bosch Center for Artificial Intelligence
Correspondence to Samuel Müller: `muellesa@cs.uni-freiburg.de`

Abstract

Currently, it is hard to reap the benefits of deep learning for Bayesian methods, which allow the explicit specification of prior knowledge and accurately capture model uncertainty. We present *Prior-Data Fitted Networks (PFNs)*. PFNs leverage in-context learning in large-scale machine learning techniques to approximate a large set of posteriors. The only requirement for PFNs to work is the ability to sample from a prior distribution over supervised learning tasks (or functions). Our method restates the objective of posterior approximation as a supervised classification problem with a set-valued input: it repeatedly draws a task (or function) from the prior, draws a set of data points and their labels from it, masks one of the labels and learns to make probabilistic predictions for it based on the set-valued input of the rest of the data points. Presented with a set of samples from a new supervised learning task as input, PFNs make probabilistic predictions for arbitrary other data points in a single forward propagation, having learned to approximate Bayesian inference. We demonstrate that PFNs can near-perfectly mimic Gaussian processes and also enable efficient Bayesian inference for intractable problems, with over 200-fold speedups in multiple setups compared to current methods. We obtain strong results in very diverse areas such as Gaussian process regression, Bayesian neural networks, classification for small tabular data sets, and few-shot image classification, demonstrating the generality of PFNs. Code and trained PFNs are released at `https://github.com/automl/TransformersCanDoBayesianInference`.

1 Introduction

In the last decade, supervised machine learning (ML) methods using deep learning architectures have made substantial progress on machine learning tasks where a large amount of training data is available (Vaswani et al., 2017; He et al., 2016; Krizhevsky et al., 2012). A very important problem in ML is thus to transfer these successes to smaller-scale setups with less data available. In this paper, we propose a way to build models that approximate posteriors with flexible and replaceable priors using deep learning models. It makes specifying a prior as simple as defining a sampling scheme of supervised learning tasks.
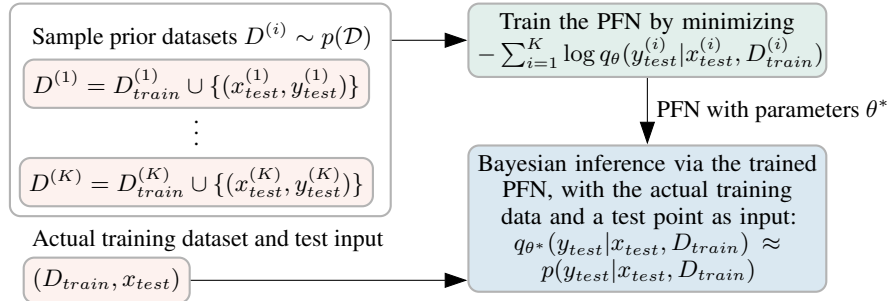

Figure 1: A visualization of Prior-Data Fitted Networks (PFNs). We sample datasets from a prior and fit a PFN on hold-out examples of these datasets. Given an actual dataset, we feed it and a test point to the PFN and obtain an approximation to Bayesian inference in a single forward propagation.

While the success of deep learning on large datasets can be attributed to the capacity of neural networks to approximate any function, there is still a need for encoding prior knowledge, for example through model architecture (e.g., Convolutional Neural Networks (LeCun et al., 1989)) or regularizers (e.g., data augmentations (Hendrycks et al., 2019; Cubuk et al., 2020)). Otherwise, the no free lunch theorems show that there are no good methods to solve the class of prediction problems (Wolpert & Macready, 1997). Thus, a large number of specialized algorithms have been developed for different small-scale tasks (LeCun et al., 1989; Kadra et al., 2021; Chen & Guestrin, 2016). Encoding prior information into a machine learning model can, however, be challenging.

A well-defined way to bias a model is to use Bayesian inference. The foundation of Bayesian inference is an assumption on the distribution of the data to appear in a real-world application. This assumption gives rise to a prior belief over the probability for the data to follow a particular model. One might, e.g., implement a prior, encoding the data as created by a neural network (Bayesian Neural Networks, (MacKay, 1992)), by a polynomial, the likelihood of a Gaussian mixture or random code in a pre-defined programming language (Solomonoff, 1997). Using Bayesian inference for prediction in supervised learning has the advantages that (i) it has a theoretical foundation that makes it valid in setups where the prior $p(t)$ fits; (ii) it can thus better account for the actual likelihood of different events; (iii) it is well calibrated and (iv) it is interpretable as the prior describes the expectations of the model. However, retrieving the posterior predictive distribution for a given prior is intractable in most cases (Blei et al., 2017; MacKay, 1992).

Figure 1 outlines Prior-Data Fitted Networks (PFNs), for approximating such Bayesian models. We assume a given representative prior distribution over supervised learning tasks (or functions), which provides our inductive bias. To train a PFN, we use supervised learning with set-valued inputs representing entire datasets: we repeatedly sample a meta-train task (or function) from the given prior, draw a set of data points and their labels from it, mask one of the labels and learn to make probabilistic predictions for it based on the set-valued input of the rest of the data points. Given an actual real-world dataset, we feed it together with a test point as inputs to the PFN and that outputs its prediction distribution for the test point, conditioned on the dataset. It performs in-context learning. As we will demonstrate, this distribution approximates exact Bayesian posterior prediction. We refer to this step as (Bayesian) inference, as opposed to the training of the PFN itself.

Our PFNs thus allow us to approximate the posterior predictive distribution for *any* prior from which we are able to sample data. This is a very weak requirement compared to the standard assumptions of other approximations for Bayesian inference (Hoffman et al., 2014; 2013; Jordan et al., 1999). This allows a simple approximation of a large set of priors, including priors that are very hard to approximate with currently available tools. We make the following contributions:

- We present architectural changes to successfully use Transformers for posterior predictive distribution (PPD) approximation, including a novel predictive distribution for regression tasks. The proposed method is simple, cheap and generally applicable to a large set of priors.
- We demonstrate that PFNs can approximate the PPD of Gaussian processes and Bayesian neural networks (BNNs) orders of magnitude faster than MCMC with NUTS or SVI with Bayes-by-Backprop (Blundell et al., 2015).
- We demonstrate that PFNs can have an impact on real-world tasks. (i) We implement BNNs with priors over architectures on PFNs that enable tuning free predictions in a single forward pass and outperform all baselines on a large benchmark of small tabular datasets. (ii) Additionally, we show that simple handwriting priors enable few-shot learning on Omniglot (Lake et al., 2015).

2 BACKGROUND

This paper concerns the use of a large amount of data to later yield strong performance on tasks for which only small datasets are available. In multiple machine learning setups, one can see successes based on this approach, such as fine-tuning unsupervised models on image data (Chen & He, 2021; Chen et al., 2020) or large language corpora (Devlin et al., 2018). Another way to transfer knowledge from large corpora is to design prompts for language models (Wang & Komatsuzaki, 2021; Brown et al., 2020). While we use a large amount of data during training, unlike the other approaches, all the data we use is generated artificially.

In meta-learning, or learning-to-learn (Hochreiter et al., 2001; Finn et al., 2017a), one tries to generalize learning methods from a training set of datasets to a validation set of datasets. Similar to our approach, there is a branch of research on building models that can learn to learn in a single forward pass (Santoro et al., 2016; Hochreiter et al., 2001; Gordon et al., 2019). More recently (Conditional) Neural Processes (Garnelo et al., 2018a;b; Kim et al., 2018) were proposed for meta-learning. These methods focus on architectural constructions as stochastic processes. The difference, besides the dissimilar model architectures and dissimilar prediction distributions, to previous meta-learning work is that we set up learning problems from which we sample artificial, on-the-fly-generated datasets such that we can show that our method does not only learn to learn, but that it learns to perform Bayesian inference.

In this work, we are interested in Bayesian posterior prediction for supervised learning problems, i.e., we model the output y for a new input x based on a supervised dataset of arbitrary size n, $\mathcal{D} = \{(x_i, y_i)\}_{i=1}^n$, where y_i is the *output* for x_i. To address the supervised learning problem in a Bayesian way, we consider a prior $p(t)$ over the latent variable t, the task. We can now use Bayes' Theorem to define the posterior $p(t|\mathcal{D})$. The crucial distribution for prediction, the posterior predictive distribution (PPD), can then be inferred as

$$p(y|x, \mathcal{D}) = \int_t p(y|x, t)p(t|\mathcal{D}). \tag{1}$$

In some cases, one can arrive at the PPD $p(y|x, \mathcal{D})$ in closed form (e.g., for Gaussian Processes, (Rasmussen & Williams, 2005)), but in most cases the PPD can only be approximated. Traditionally, one approximates the posterior $p(t|\mathcal{D})$ and based on this approximation infers an approximation of the PPD. To approximate the posterior, there are two classes of prominent methods: i) Markov Chain Monte Carlo (MCMC) (Neal, 1996; Andrieu et al., 2003; Welling & Teh, 2011) methods, like NUTS (Hoffman et al., 2014), allow accurate but sometimes very slow approximations of the posterior; and ii) Variational Inference (VI) (Jordan et al., 1999; Wainwright & Jordan, 2008; Hoffman et al., 2013) methods approximate the posterior by a tractable distribution, such as a factorized normal distribution.

One more related line of research is amortized simulation-based inference (Cranmer et al., 2020; Chan et al., 2018), which was previously adapted to general probabilistic programs (Ritchie et al., 2016) and sequences (Ortega et al., 2019). In particular relevant to this work is neural posterior estimation (Lueckmann et al., 2021; Papamakarios & Murray, 2016). The objective here is to find a model that approximates the posterior $p(t|X)$ by training on samples from $p(t, X)$, where X can be a dataset $\mathcal{D}$ like above, but typically is a single vector. Previous work in simulation-based inference is focused on simulations for which a specific model underlying the data is known (Lueckmann et al., 2021). Our method is in so far similar to simulation-based inference as both solely use samples from the prior. In the next section, we will show how we can model the PPD directly, though, without ever instantiating the posterior, and apply this to large datasets with general priors.

3 PPD APPROXIMATION WITH PFNS

Let us consider a parameterized model q_θ that can accept a dataset $D = \{(x_i, y_i)\}_{i=1}^n$, as well as a query x as input, and which predicts a distribution over possible values of y for the query x. Many neural architectures can be used as such a model; in this paper, we use a variant of Transformers

---

Algorithm 1: Training a PFN model by Fitting Prior-Data

Input : A prior distribution over datasets $p(\mathcal{D})$, from which samples can be drawn and the number of samples K to draw
Output : A model q_θ that will approximate the PPD
Initialize the neural network q_θ;
for $j \leftarrow 1$ **to** K **do**
$\quad$ Sample $D \cup \{(x_i, y_i)\}_{i=1}^m \sim p(\mathcal{D})$;
$\quad$ Compute stochastic loss approximation $\bar{\ell}_\theta = \sum_{i=1}^m (-\log q_\theta(y_i|x_i, D))$;
$\quad$ Update parameters θ with stochastic gradient descent on $\nabla_\theta \bar{\ell}_\theta$;
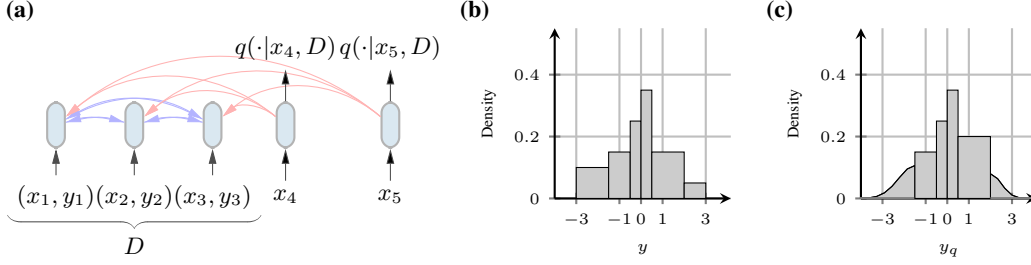**end**

Figure 2: (a) A visualization of the Transformer for $n = 3$ input pairs and $m = 2$ queries. Every bar is the representation of one input and the arrows show what each representation can attend to. (b-c) A visualisation of the Riemann distribution, with and without bounded support.

(Vaswani et al., 2017) as they are a reliable and powerful architecture. We train this model by cross-entropy over samples drawn from the prior. Our proposed loss, the *Prior-Data Negative Log-Likelihood (Prior-Data NLL)* ℓ_θ is defined as

$$\ell_\theta = \mathbb{E}_{D \cup \{x,y\} \sim p(\mathcal{D})}[-\log q_\theta(y|x, D)], \tag{2}$$

where $D \cup \{x, y\}$ simply is a dataset of size $|D| + 1$ sampled from $p(\mathcal{D})$.

PFNs are trained to minimize ℓ_θ like outlined in Algorithm 1: We draw many datasets from our prior and fit our model to predict a hold-out example correctly for these.

In contrast to VI and MCMC, we learn to approximate the PPD directly from dataset samples. For all cases we consider, it is simple and cheap to sample from $p(\mathcal{D})$, fulfilling the only requirement our method has. MCMC on the other hand requires access to a non-normalized posterior $f(t|D, x) \propto p(t|D, x)$, and VI requires access to the density values of $p(t, D)$, both of which can be hard to compute.

Extending standard loss derviations Gordon et al. (2019) to the meta-level, we can show that minimizing the Prior-Data NLL ℓ_θ yields an approximation of the PPD in terms of cross-entropy and thus *KL*-Divergence:

Insight 1. *The proposed objective ℓ_θ is equal to the expectation of the cross-entropy between the PPD and its approximation q_θ: $\ell_\theta = \mathbb{E}_{x,D \sim p(\mathcal{D})}[H(p(\cdot|x, D), q_\theta(\cdot|x, D))]$*

Proof. The above can be shown with a simple derivation. We mark transformations for easy reading.

$$\ell_\theta = -\int_{D,x,y} p(x, y, D) \log q_\theta(y|x, D) = -\int_{D,x} p(x, D) \int_y p(y|x, D) \log q_\theta(y|x, D) \tag{3}$$

$$= \int_{D,x} p(x, D) \mathrm{H}(p(\cdot|x, D), q_\theta(\cdot|x, D)) = \mathbb{E}_{x,D \sim p(\mathcal{D})}[\mathrm{H}(p(\cdot|x, D), q_\theta(\cdot|x, D))] \tag{4}$$

$\square$

Thus, we have an approximation of the PPD. We can formulate this in terms of *KL*-Divergence, too.

Corollary 1.1. *The loss ℓ_θ equals the expected KL-Divergence $\mathbb{E}_{D,x}[KL(p(\cdot|x, D), q_\theta(\cdot|x, D))]$ between $p(\cdot|x, D)$ and $q_\theta(\cdot|x, D)$ over prior data x, D, up to an additive constant. Proof in App. A.*

In the following, we consider the optimum of the given optimization problem $\theta^* \in \arg\min_\theta \ell_\theta$.

Corollary 1.2. *If p is a member of the distribution family q_θ (i.e., there is a θ such that $q_\theta = p$), we have $q_{\theta^*}(\cdot|x, D) = p(\cdot|x, D)$ for all x, D for which $p(\cdot|x, D)$ is defined. Proof in App. B.*[1]

---

[1]Update (2024): This finding was first published by Foong et al. (2020) in Section 3.2 Prop. 1.
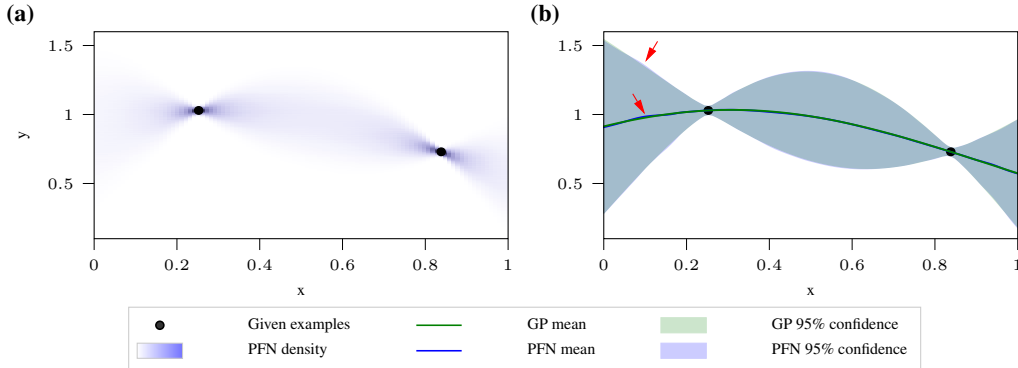
Figure 3: (a) The PFN's PPD given two evaluations of the function, highlighting the binning it its predictions (best viewed in full-screen mode). (b) The PFN's and the GP's mean and confidence intervals, which are nearly identical (red arrows mark tiny exemplary differences). For additional comparisons, see Figure 7 in the appendix.

4 ADAPTING THE TRANSFORMER FOR BAYESIAN INFERENCE

In this section, we propose an efficient architecture based on the Transformer encoder (Vaswani et al., 2017) and a novel regression head for regression problems.

An Efficient Architecture Our architecture, visualized in Figure 2a, is based on a Transformer encoder without positional encodings, which makes it invariant to permutations in the dataset D. We feed the Transformer with simple linear projections of our inputs and queries. Our model returns the PPD for each given query x, only depending on the dataset D and the query itself. We sample the number of inputs n and queries m randomly such that $N = m + n$ for some fixed N. See Appendix E.1 for a more detailed description and Appendix E.3 for an ablation of the permutation invariance. For additional practical training information see Appendix D.

Riemann Distribution The modelling of continuous distributions is hard with neural networks. To yield strong performance in modelling PPDs, we used a distribution that works particularly well with neural networks. Based on the knowledge that neural networks work well for classification and inspired by discretizations in distributional reinforcement learning (Bellemare et al., 2017), we made use of a discretized continuous distribution that we call *Riemann Distribution*. PDFs of this distribution are bar plots, see Figure 2b. We select the boundaries of the buckets **B** in which we discretize such that they all have the same probability in prior-data: $p(y \in b) = 1/|\mathbf{B}|, \forall b \in \mathbf{B}$. We estimate this using a large prior-data sample. In experiments with priors that need unbounded support, we replace the last bar on each side with an appropriately scaled half-normal distribution, see Figure 2c. For a more exact definition, we refer the reader to Appendix E.2. For an ablation of the Riemann distribution, see Appendix E.3.

Theorem 1. *A Riemann distribution $q_{\mathbf{B}}$ with finite support, where $\mathbf{B}$ are the buckets, can model any distribution with a finite, almost everywhere continuous (Riemann-integrable) density function and full support up to arbitrary precision. That is, $\forall p \forall \epsilon \exists \mathbf{B}.KL(q_{\mathbf{B}}, p) \leq \epsilon$. Proof in App. C.*

5 POSTERIOR APPROXIMATION STUDIES

In our first set of experiments, we study the capability of PFNs to perform Bayesian inference for the tractable case of Gaussian Processes (GPs) with fixed hyperparameters (where we can compare to ground truth data; Section 5.1) and the intractable cases of GPs with unknown hyperparameters (Section 5.2) and Bayesian Neural Networks (BNNs; Section 5.3).

Corollary 1.1 shows that the Prior-Data NLL is equal to the *KL*-Divergence between the exact PPD and the approximation, up to an additive constant. We thus use it in all following experiments to compare how close methods can match the correct PPD. For methods that do not approximate the PPD directly, we approximate the integral of the PPD in Equation 1 with a large Monte Carlo integration. In this section, we report the 95% confidence interval over different sampled datasets of
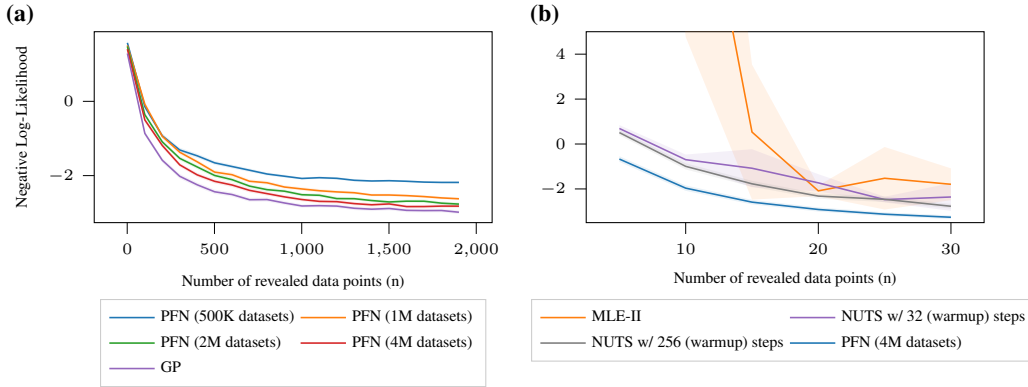
Figure 4: (a) Prior-Data NLL with a fixed GP. While, the PPD of the GP is exact, we can see that our approximations get very close to it. (b) Prior-Data NLL with a mix over GP hyperparameters. There is no closed-form solution for this PPD, but we can see that our PFN still gets closest to the true PPD. Our PFN is also more than $200\times$ faster than any of the baselines.

the Prior-Data NLL for each experiment as shaded areas alongside the mean. We refer the reader to Appendix F for more information on the setup.

5.1 GAUSSIAN PROCESS APPROXIMATION

We begin by approximating GPs to study what PFNs are capable of; GPs with fixed hyperparameters are convenient for this purpose since the tractability of their PPD allows us to assess how close our approximation is to the exact PPD. To create the prior for this task, we sample the N inputs x_i uniformly at random from the unit-cube. The data-prior of a zero-mean GP with a kernel function k, given the x_i's, can be described as a multivariate normal distribution $\mathcal{N}(\mathbf{0}, K)$, where $K_{i,j} = k(x_i, x_j)$. We sample from this normal distribution to yield a dataset $\{(x_1, y_1), \ldots, (x_N, y_N)\}$. As described above, we then train our PFNs to predict the y's for a held-out subset of the dataset. The trained PFN can then be used to approximate the PPD for new datasets and arbitrary query points in the unit-cube.

Figure 3 visualizes the predictions of such a PFN with two data points and query points x ranging from 0 to 1. We visualize both the estimated PPD as a heat map, as well as confidence bounds, compared to the exact PPD. The estimated confidence intervals and means are virtually indistinguishable from the ground truth, therefore we marked the most noticeable differences with red arrows. The model learns on its own, completely automatically, to generate smooth distributions without any explicit knowledge of the positions of the bars in $\mathbb{R}$. We published[2] an interactive version of this experiment. In Figure 7 of the appendix, we show more qualitative examples of the behavior of our approximation together with the exact posterior for a different length scale. In Figure 8, we additionally compare to Attentive Neural Processes (Kim et al., 2018), showing the clear superiority of our method for Bayesian Inference. Figure 4a shows that the qualitative results above generalize to datasets with up to 2000 examples with multiple features. The tractable GP posterior, which achieves optimal performance by definition, is approximated very closely, and increasingly better so the more meta-train datasets we train the PFN for.

5.2 APPROXIMATING A GP WITH HYPER-PRIORS

A common practice in fields applying GPs in the real world is to define distributions over the hyperparameters of these GPs (Rasmussen & Williams, 2006; Snoek et al., 2012), so-called hyper-priors. Thus, the prior of these models considers a more diverse set of functions, to model the fact that the correlation between data points, the smoothness of functions and the scale of outputs varies across applications. The downside of using hyper-priors is that it is not possible to compute the PPD of the GP exactly anymore. There are two common practices to approximate it anyways, and we evaluate

---

[2] https://huggingface.co/spaces/samuelinferences/transformers-can-do-bayesian-inference
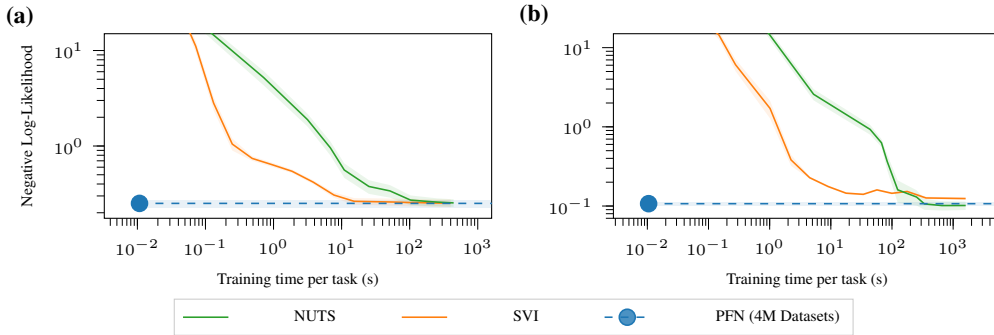
(a)

(b)

Figure 5: Time spent for Bayesian Inference per dataset compared to Prior-Data NLL. For NUTS we scale the number of warmup and sampling steps, for SVI, we scale the number of training steps and averaged samples. PFN is evaluated at only one setting (blue dot). We show two different BNN architectures (a) a BNN with 3 features, 2 layers and a hidden dimensionality of 5 and (b) a BNN with 8 features, 2 layers and a hidden dimensionality of 64.

against both. (i) Firstly, MLE-II, the most common approximation. This is a simple special case of variational inference. Here, suitable hyperparameters are found by maximum a posteriori (MAP) estimation (e.g., Rasmussen & Williams (2006)). We use the fitting setup of BoTorch (Balandat et al., 2020) which also inspired our hyper-priors. (ii) Secondly, Markov Chain Monte Carlo (MCMC), a method to sample from any distribution for which one can calculate non-normalized probabilities, that is also frequently applied to sample hyperparameters (e.g., Snoek et al. (2012)). Here, we use the state-of-the-art algorithm NUTS (Hoffman et al., 2014), which uses gradients to facilitate the Hamiltonian Monte Carlo algorithm. We plot the performance of the different methods in Figure 4b. Our model can approximate the PPD on the prior much closer than both of these methods, and its inference is more than $200\times$ faster than MLE-II and $1\,000\times$ to $8\,000\times$ faster than NUTS. Further details can be found in Appendix F.

5.3 APPROXIMATING BNNS

Bayesian Neural Networks (BNNs) provide a strong ability to model uncertainty due to their Bayesian nature, compared to traditional neural networks. Recently, posterior approximation methods, such as stochastic variational inference (SVI) and stochastic gradient MCMC methods (such as NUTS) allow for much faster convergence, which has sparked a lot of interest in the area (Izmailov et al., 2021; Fortuin et al., 2021). However, computational feasibility still remains a key issue of current BNNs.

In Figure 5, we show that our PFNs can outperform today's default methods for BNN inference using a fraction of their compute budget (PFNs are $1\,000\times$ faster than Bayes-by-Backprop SVI and $10\,000\times$ faster than NUTS to achieve the same performance). The figure shows the Prior-Data NLL of the BNN prior that is used during inference by all solvers. To generate prior-data for our PFNs, we sampled random weights for a BNN Φ and used normally-distributed i.i.d. feature vectors X_i to obtain $y_i := \Phi(X_i)$ with $\mathcal{D} := (X_{1:n}, y_{1:n})$. For the evaluation we sampled 100 datasets, with $m = 200$ test data points and $n = 100$ revealed data points per dataset. A detailed description of baselines as well as further experiments are included in Appendix F.

6 APPLICATION TO TABULAR DATASETS

We evaluate Transformer-based classifiers with priors over Gaussian Processes and Bayesian Neural Networks on a range of small real-world tabular datasets. Surprisingly, the simple priors we describe next outperform a large set of baselines, including XGB (Chen & Guestrin, 2016) and Catboost (Prokhorenkova et al., 2018), while greatly surpassing all baselines in uncertainty calibration.

A GP Prior for Tabular Classification We build a classification prior based on GPs with a hyper-prior, as described in Section 5.2. Before, we used this prior for regression. To make it a classification prior, we find the median over all targets in the dataset y and set the class to one if greater than the median and zero otherwise.
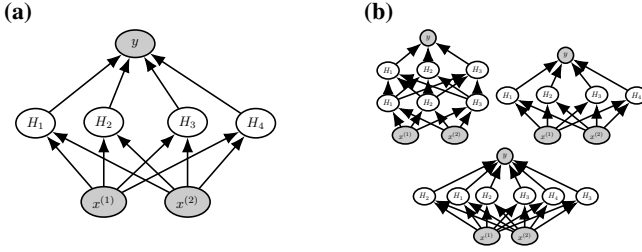
(a)

(b)

Figure 6: (a) A BNN. The inputs x are mapped to the output y. (b) A prior over BNN architectures. The network considers a distribution over different model architectures at once.

A BNN Prior over Architectures We generalize our BNN setup to learn a prior over model architectures. Fitting a neural network requires finding a suitable architecture, e.g., embedding size, number of layers and activation function. Commonly, resource-intensive searches need to be employed to find suitable architectures (Liu et al., 2018; Zoph et al., 2018). The result of this search is not a posterior distribution over architecture choices and their respective parameters, though, but instead only a point-estimate of the architecture choice. This is true for Bayesian optimisation approaches as well (Kandasamy et al., 2019; Zhou et al., 2019; Ru et al., 2021). Ensembling methods over multiple architectures can yield a rough approximation to a distribution over architectures, but this scales linearly in cost with the number of architectures considered (Zaidi et al., 2020). Using dropout can be regarded as ensemble learning but is limited to varying connectivity (Hara et al., 2017). PFNs allow us to be fully Bayesian, not only about the weights of the BNN, but its architecture, too. By defining a prior probability over the space of model architectures, we remove the need for finding an optimal neural architecture and instead jointly integrate over the space of architectures and their respective weights in a single Bayesian inference. This yields a distribution over architectures in the posterior. The degrees of freedom of model architectures we considered can be found in Appendix G. Our prior-data sampling algorithm for learning to predict based on a prior over both weights and architectures iterates the following steps:

(1) Sample a model architecture $A \sim p(A)$
(2) Sample model weights for the given architecture: $W_{i,j} \sim p_w(\cdot)$
(3) Sample i.i.d. features $x_{i,f} \sim \mathcal{N}(0,1)$ for each data point i and each feature f
(4) Propagate each x_i forward through A_W yielding $\{(x_i, A_W(x_i))\}_{i=1}^N$

We binarized targets like for the GP Prior above. See Appendix G for more details.

Setup of Datasets We used a large collection of tabular datasets from the open-source OpenML AutoML Benchmark (Gijsbers et al., 2019); we first removed datasets with more than one hundred features or missing values, ending up with 20 datasets that represent a diverse set of classification problems with numerical and categorical features. We then simplified each dataset to a balanced binary classification problem, and, for each dataset sampled 20 subsets, each including 100 samples. Within each subset we provide labels for the first 30 samples and evaluate on the remaining samples. All baselines and PFNs use the same datasets and subsets. We also define a set of six unrelated validation datasets used for optimizing the prior distribution over architectures of the PFNs. This is similar to setting the range of hyperparameters in a cross-validation grid search and can be reused for all similar problems. See Appendix G for more details.

Setup of Models Our baselines comprise two Gradient Boosted Tree algorithms, XGBoost (Chen & Guestrin, 2016) and Catboost (Prokhorenkova et al., 2018), as well as logistic regression, K-Nearest Neighbors, Gaussian Processes (RBF Kernel) and Bayesian Neural Networks (Bayes-by-Backprop SVI with Pyro). Catboost additionally received information on which features are categorical. We used two PFNs, one PFN for each prior described above. We were able to apply the same model across different feature dimensions. We used grid search with 5-fold cross-validation to optimize our baselines' hyperparameters for each dataset, using the hyperparameter spaces described in Table 6 in the appendix.

Experimental Results Table 1 compares the area under the receiver operating curve (ROC AUC) of PFNs based on BNN and GP priors against the various baselines. While the PFN-GP demonstrates on-par performance to the best of the evaluated baselines, the PFN-BNN performs strongest in this comparison. The Wilcoxon signed-rank test (Demšar, 2006), a standard metric for comparing classifiers across multiple datasets is evaluated on each of the 20 subsets of the 21 evaluation datasets separately and shows a significant performance improvement. While all baselines make use of cross-validation to find suitable hyperparameters, the PFNs naturally consider a distribution of

Metric	PFN-BNN	PFN-GP	Log. Reg.	GP	KNN	BNN	Catboost	XGB
Mean rank ROC AUC	**2.786**	3.833	4.690	5.286	6.214	5.000	4.833	3.357
Loss/Tie/Win vs PFN-BNN	–	14/1/6	16/1/4	17/0/4	17/1/3	17/1/3	13/1/7	12/2/7
Wilcoxon p. vs PFN-BNN	–	3.6e-13	3.6e-13	3.9e-13	3.6e-13	3.6e-13	1.9e-12	1.6e-06
Expected Calibration Error	**0.025**	0.067	0.157	0.095	0.093	0.089	0.157	0.066
Benchmark Time	GPU: **0:00:13** CPU: 0:04:23		0:09:56	0:24:30	0:00:34	12:04:41	2:05:20	20:59:46

Table 1: Aggregated performance on subsets of datasets with 30 training samples. Our novel PFN-BNN performs strongest overall. See Table 7 in the appendix for per-dataset results.

hyperparameters and integrate cross-validation and training within the model's Bayesian inference step. As shown in Table 1, this makes it very fast compared to the baselines: since all it needs to do on a new dataset is a single forward propagation step, when run on a GPU (Nvidia Tesla V100), it requires as little as 13 seconds for all 20 datasets combined. This is more than $5000\times$ faster than the 20 hours XGBoost requires, and even faster than K-Nearest Neighbors.

We can also experimentally confirm that our PFNs make well-adjusted uncertainty predictions. We find that on our data they have lower Expected Calibration Error (ECE, using 100 bins (Naeini et al., 2015)) even than standard BNNs and ensemble methods such as XGBoost, the two baseline methods that best capture uncertainty. We also provide confidence histograms in Figure 10 of the appendix, visually demonstrating the PFN's strong calibration.

7 APPLICATION TO FEW-SHOT LEARNING

As shown in the previous section, PFNs can be trained with priors that are not (easily) possible to use in the traditional Bayesian setups. In this section, we show another example of this, building a prior for hand-written digits and letters and demonstrating strong performance on Omniglot (Lake et al., 2015) in combination with fine-tuning of the PFN on Omniglot.

As an approximation to hand-written symbols, we create a prior that generates random straight lines. In each sample from this prior, we consider five different random line assortments as class prototypes. For each instance of a class, we apply noise to the positions of the lines. It required just 55 lines of readable code to create this prior (see Figure 11 in the Appendix). In Figure 12 of the Appendix we show a sample dataset from this prior.

For our evaluation on Omniglot, we follow the setup of Rothfuss et al. (2021). We perform 5-shot 5-way classification, i.e. we consider five classes and five examples of each class. We create one task from the first five classes of each of the 30 train and 20 evaluation alphabets in Omniglot. We train our PFN on the synthetic prior and then fine-tune it on the 30 training tasks created. This practice is unlike the previous sections. Our premise is to show the flexibility of our model: it can even be fine-tuned on similar datasets, if these are available. We do not use task augmentation, like Rothfuss et al. (2021), but apply translations to each image, as we only use simple linear layers to encode the images in the Transformer. In Table 2 one can see that for this very hard version of the Omniglot dataset our simple method yields results on par with the state of the art. For more information on the setup, please see Appendix H.

Method	Accuracy	Method	Accuracy
Vanilla BNN (Liu & Wang, 2016)	0.795 ± 0.006	MLAP (Amit & Meir, 2018)	0.700 ± 0.0135
MAML (Finn et al., 2017b)	0.693 ± 0.013	BMAML (Yoon et al., 2018)	0.764 ± 0.025
PACOH-NN (Rothfuss et al., 2021)	$\mathbf{0.885 \pm 0.090}$	PFN (this work)	$\mathbf{0.865 \pm 0.019}$

Table 2: Comparison of meta-learning algorithms in terms of test accuracy on the Omniglot dataset. Results within the confidence interval of the best performance are bold-faced.

8 CONCLUSION & FUTURE WORK

We presented Prior-Fitted Networks (PFNs), a novel way to efficiently approximate the posterior predictive distribution using deep neural networks and showed its capability on a set of diverse tasks and priors. We expect the following future work to be especially fruitful: (i) Work on finding novel priors that are now feasible to approximate using PFNs. (ii) Work on architectures that are well-fit for this task, as we simply used a slight adaption of current Transformer models. (iii) Work on scaling PFNs to even larger real-world problems. (iv) Work on using our model for the amortized simulation-based inference setting.

9 ACKNOWLEDGEMENTS

REFERENCES

Ron Amit and Ron Meir. Meta-learning by adjusting priors based on extended pac-bayes theory. In *International Conference on Machine Learning*, pp. 205–214. PMLR, 2018.

Christophe Andrieu, Nando De Freitas, Arnaud Doucet, and Michael I Jordan. An introduction to mcmc for machine learning. *Machine learning*, 50(1):5–43, 2003.

Maximilian Balandat, Brian Karrer, Daniel R. Jiang, Samuel Daulton, Benjamin Letham, Andrew Gordon Wilson, and Eytan Bakshy. BoTorch: A Framework for Efficient Monte-Carlo Bayesian Optimization. In *Advances in Neural Information Processing Systems 33*, 2020.

Marc G Bellemare, Will Dabney, and Rémi Munos. A distributional perspective on reinforcement learning. In *International Conference on Machine Learning*, pp. 449–458. PMLR, 2017.

Eli Bingham, Jonathan P. Chen, Martin Jankowiak, Fritz Obermeyer, Neeraj Pradhan, Theofanis Karaletsos, Rohit Singh, Paul Szerlip, Paul Horsfall, and Noah D. Goodman. Pyro: Deep Universal Probabilistic Programming. *Journal of Machine Learning Research*, 2018.

David M. Blei, Alp Kucukelbir, and Jon D. McAuliffe. Variational inference: A review for statisticians. *Journal of the American Statistical Association*, 112(518):859–877, Apr 2017. ISSN 1537-274X. doi: 10.1080/01621459.2017.1285773.

C Blundell, J. Cornebise, K. Kavukcuoglu, and D. Wierstra. Weight uncertainty in neural network. In F. Bach and D. Blei (eds.), *Proceedings of the 32nd International Conference on Machine Learning (ICML'15)*, volume 37, pp. 1613–1622. Omnipress, 2015.

Tom B Brown, Benjamin Mann, Nick Ryder, Melanie Subbiah, Jared Kaplan, Prafulla Dhariwal, Arvind Neelakantan, Pranav Shyam, Girish Sastry, Amanda Askell, et al. Language models are few-shot learners. *arXiv preprint arXiv:2005.14165*, 2020.

Jeffrey Chan, Valerio Perrone, Jeffrey P Spence, Paul A Jenkins, Sara Mathieson, and Yun S Song. A likelihood-free inference framework for population genetic data using exchangeable neural networks. In *NeurIPS*, 2018.

Tianqi Chen and Carlos Guestrin. Xgboost: A scalable tree boosting system. In *Proceedings of the 22nd ACM SIGKDD International Conference on Knowledge Discovery and Data Mining*, KDD '16, pp. 785–794, New York, NY, USA, 2016. Association for Computing Machinery. ISBN 9781450342322. doi: 10.1145/2939672.2939785.

Ting Chen, Simon Kornblith, Mohammad Norouzi, and Geoffrey Hinton. A simple framework for contrastive learning of visual representations. In *International conference on machine learning*, pp. 1597–1607. PMLR, 2020.

Xinlei Chen and Kaiming He. Exploring simple siamese representation learning. In *Proceedings of the IEEE/CVF Conference on Computer Vision and Pattern Recognition*, pp. 15750–15758, 2021.

Kyle Cranmer, Johann Brehmer, and Gilles Louppe. The frontier of simulation-based inference. *Proceedings of the National Academy of Sciences*, 117(48):30055–30062, 2020.

Ekin D Cubuk, Barret Zoph, Jonathon Shlens, and Quoc V Le. Randaugment: Practical automated data augmentation with a reduced search space. In *Proceedings of the IEEE/CVF Conference on Computer Vision and Pattern Recognition Workshops*, pp. 702–703, 2020.

Janez Demšar. Statistical comparisons of classifiers over multiple data sets. *J. Mach. Learn. Res.*, 7: 1–30, December 2006. ISSN 1532-4435.

Jacob Devlin, Ming-Wei Chang, Kenton Lee, and Kristina Toutanova. Bert: Pre-training of deep bidirectional transformers for language understanding. *arXiv preprint arXiv:1810.04805*, 2018.

C. Finn, P. Abbeel, and S. Levine. Model-agnostic meta-learning for fast adaptation of deep networks. In D. Precup and Y. Teh (eds.), *Proceedings of the 34th International Conference on Machine Learning (ICML'17)*, volume 70, pp. 1126–1135. Proceedings of Machine Learning Research, 2017a.

C. Finn, T. Yu, T. Zhang, P. Abbeel, and S. Levine. One-shot visual imitation learning via meta-learning. In *Proceedings of the 1st Annual Conference on Robot Learning (CoRL)*, volume 78, pp. 357–368. PMLR, 2017b.

Andrew Foong, Wessel Bruinsma, Jonathan Gordon, Yann Dubois, James Requeima, and Richard Turner. Meta-learning stationary stochastic process prediction with convolutional neural processes. *Advances in Neural Information Processing Systems*, 33:8284–8295, 2020.

Vincent Fortuin, Adrià Garriga-Alonso, Florian Wenzel, Gunnar Rätsch, Richard Turner, Mark van der Wilk, and Laurence Aitchison. Bayesian neural network priors revisited, 2021.

Marta Garnelo, Dan Rosenbaum, Christopher Maddison, Tiago Ramalho, David Saxton, Murray Shanahan, Yee Whye Teh, Danilo Rezende, and SM Ali Eslami. Conditional neural processes. In *International Conference on Machine Learning*, pp. 1704–1713. PMLR, 2018a.

Marta Garnelo, Jonathan Schwarz, Dan Rosenbaum, Fabio Viola, Danilo J Rezende, SM Eslami, and Yee Whye Teh. Neural processes. *arXiv preprint arXiv:1807.01622*, 2018b.

P. Gijsbers, E. LeDell, S. Poirier, J. Thomas, B. Bischl, and J. Vanschoren. An open source automl benchmark. *arXiv preprint arXiv:1907.00909 [cs.LG]*, 2019. Accepted at AutoML Workshop at ICML 2019.

Jonathan Gordon, John Bronskill, Matthias Bauer, Sebastian Nowozin, and Richard Turner. Meta-learning probabilistic inference for prediction. In *International Conference on Learning Representations*, 2019.

Kazuyuki Hara, Daisuke Saitoh, and Hayaru Shouno. Analysis of dropout learning regarded as ensemble learning. *CoRR*, abs/1706.06859, 2017.

Kaiming He, Xiangyu Zhang, Shaoqing Ren, and Jian Sun. Deep residual learning for image recognition. In *Proceedings of the IEEE conference on computer vision and pattern recognition*, pp. 770–778, 2016.

Dan Hendrycks, Norman Mu, Ekin Dogus Cubuk, Barret Zoph, Justin Gilmer, and Balaji Lakshminarayanan. Augmix: A simple data processing method to improve robustness and uncertainty. In *International Conference on Learning Representations*, 2019.

Sepp Hochreiter, A Steven Younger, and Peter R Conwell. Learning to learn using gradient descent. In *International Conference on Artificial Neural Networks*, pp. 87–94. Springer, 2001.

Matthew D. Hoffman, David M. Blei, Chong Wang, and John Paisley. Stochastic variational inference. *Journal of Machine Learning Research*, 14(4):1303–1347, 2013.

Matthew D Hoffman, Andrew Gelman, et al. The no-u-turn sampler: adaptively setting path lengths in hamiltonian monte carlo. *J. Mach. Learn. Res.*, 15(1):1593–1623, 2014.

Pavel Izmailov, Sharad Vikram, Matthew D. Hoffman, and Andrew Gordon Wilson. What are bayesian neural network posteriors really like? *CoRR*, abs/2104.14421, 2021.

Michael I Jordan, Zoubin Ghahramani, Tommi S Jaakkola, and Lawrence K Saul. An introduction to variational methods for graphical models. *Machine learning*, 37(2):183–233, 1999.

Arlind Kadra, Marius Lindauer, Frank Hutter, and Josif Grabocka. Regularization is all you need: Simple neural nets can excel on tabular data, 2021.

Kirthevasan Kandasamy, Willie Neiswanger, Jeff Schneider, Barnabas Poczos, and Eric Xing. Neural architecture search with bayesian optimisation and optimal transport, 2019.

Hyunjik Kim, Andriy Mnih, Jonathan Schwarz, Marta Garnelo, Ali Eslami, Dan Rosenbaum, Oriol Vinyals, and Yee Whye Teh. Attentive neural processes. In *International Conference on Learning Representations*, 2018.

Diederik P Kingma and Jimmy Ba. Adam: A method for stochastic optimization. In *ICLR (Poster)*, 2015.

Alex Krizhevsky, Ilya Sutskever, and Geoffrey E Hinton. Imagenet classification with deep convolutional neural networks. In F. Pereira, C. J. C. Burges, L. Bottou, and K. Q. Weinberger (eds.), *Advances in Neural Information Processing Systems*, volume 25. Curran Associates, Inc., 2012.

Brenden M Lake, Ruslan Salakhutdinov, and Joshua B Tenenbaum. Human-level concept learning through probabilistic program induction. *Science*, 350(6266):1332–1338, 2015.

Y. LeCun, B. Boser, J. S. Denker, D. Henderson, R. E. Howard, W. Hubbard, and L. D. Jackel. Backpropagation applied to handwritten zip code recognition. *Neural Computation*, 1(4):541–551, 1989. doi: 10.1162/neco.1989.1.4.541.

Hanxiao Liu, Karen Simonyan, and Yiming Yang. Darts: Differentiable architecture search. In *International Conference on Learning Representations*, 2018.

Qiang Liu and Dilin Wang. Stein variational gradient descent: A general purpose bayesian inference algorithm. *arXiv preprint arXiv:1608.04471*, 2016.

Ilya Loshchilov and Frank Hutter. Sgdr: Stochastic gradient descent with warm restarts. *arXiv preprint arXiv:1608.03983*, 2016.

Jan-Matthis Lueckmann, Jan Boelts, David Greenberg, Pedro Goncalves, and Jakob Macke. Benchmarking simulation-based inference. In *International Conference on Artificial Intelligence and Statistics*, pp. 343–351. PMLR, 2021.

David JC MacKay. A practical bayesian framework for backpropagation networks. *Neural Computation*, 4(3):448–472, 1992.

Mahdi Pakdaman Naeini, Gregory F. Cooper, and Milos Hauskrecht. Obtaining well calibrated probabilities using bayesian binning. In *Proceedings of the Twenty-Ninth AAAI Conference on Artificial Intelligence*, AAAI'15, pp. 2901–2907. AAAI Press, 2015. ISBN 0262511290.

R. Neal. *Bayesian Learning for Neural Networks*. 1996.

Pedro A Ortega, Jane X Wang, Mark Rowland, Tim Genewein, Zeb Kurth-Nelson, Razvan Pascanu, Nicolas Heess, Joel Veness, Alex Pritzel, Pablo Sprechmann, et al. Meta-learning of sequential strategies. *arXiv preprint arXiv:1905.03030*, 2019.

George Papamakarios and Iain Murray. Fast ε-free inference of simulation models with bayesian conditional density estimation. In *Advances in neural information processing systems*, pp. 1028–1036, 2016.

Adam Paszke, Sam Gross, Francisco Massa, Adam Lerer, James Bradbury, Gregory Chanan, Trevor Killeen, Zeming Lin, Natalia Gimelshein, Luca Antiga, Alban Desmaison, Andreas Kopf, Edward Yang, Zachary DeVito, Martin Raison, Alykhan Tejani, Sasank Chilamkurthy, Benoit Steiner, Lu Fang, Junjie Bai, and Soumith Chintala. Pytorch: An imperative style, high-performance deep learning library. In H. Wallach, H. Larochelle, A. Beygelzimer, F. d'Alché-Buc, E. Fox, and R. Garnett (eds.), *Advances in Neural Information Processing Systems 32*, pp. 8024–8035. Curran Associates, Inc., 2019.

Liudmila Prokhorenkova, Gleb Gusev, Aleksandr Vorobev, Anna Veronika Dorogush, and Andrey Gulin. Catboost: Unbiased boosting with categorical features. In *Proceedings of the 32nd International Conference on Neural Information Processing Systems*, NIPS'18, pp. 6639–6649, Red Hook, NY, USA, 2018. Curran Associates Inc.

C. Rasmussen and C. Williams. *Gaussian Processes for Machine Learning*. The MIT Press, 2006.

Carl Edward Rasmussen and Christopher K. I. Williams. *Gaussian Processes for Machine Learning (Adaptive Computation and Machine Learning)*. The MIT Press, 2005. ISBN 026218253X.

Daniel Ritchie, Paul Horsfall, and Noah D Goodman. Deep amortized inference for probabilistic programs. *arXiv preprint arXiv:1610.05735*, 2016.

Jonas Rothfuss, Vincent Fortuin, Martin Josifoski, and Andreas Krause. Pacoh: Bayes-optimal meta-learning with pac-guarantees. In *International Conference on Machine Learning*, pp. 9116–9126. PMLR, 2021.

Binxin Ru, Xingchen Wan, Xiaowen Dong, and Michael Osborne. Interpretable neural architecture search via bayesian optimisation with weisfeiler-lehman kernels. In *International Conference on Learning Representations*, 2021.

Adam Santoro, Sergey Bartunov, Matthew Botvinick, Daan Wierstra, and Timothy Lillicrap. Meta-learning with memory-augmented neural networks. In *International conference on machine learning*, pp. 1842–1850. PMLR, 2016.

J. Snoek, H. Larochelle, and R. Adams. Practical Bayesian optimization of machine learning algorithms. In P. Bartlett, F. Pereira, C. Burges, L. Bottou, and K. Weinberger (eds.), *Proceedings of the 25th International Conference on Advances in Neural Information Processing Systems (NeurIPS'12)*, pp. 2960–2968, 2012.

Ray J Solomonoff. The discovery of algorithmic probability. *Journal of Computer and System Sciences*, 55(1):73–88, 1997. ISSN 0022-0000. doi: https://doi.org/10.1006/jcss.1997.1500.

Ashish Vaswani, Noam Shazeer, Niki Parmar, Jakob Uszkoreit, Llion Jones, Aidan N Gomez, Ł ukasz Kaiser, and Illia Polosukhin. Attention is all you need. In I. Guyon, U. V. Luxburg, S. Bengio, H. Wallach, R. Fergus, S. Vishwanathan, and R. Garnett (eds.), *Advances in Neural Information Processing Systems*, volume 30. Curran Associates, Inc., 2017.

Martin J Wainwright and Michael Irwin Jordan. *Graphical models, exponential families, and variational inference*. Now Publishers Inc, 2008.

Ben Wang and Aran Komatsuzaki. GPT-J-6B: A 6 Billion Parameter Autoregressive Language Model. `https://github.com/kingoflolz/mesh-transformer-jax`, May 2021.

Max Welling and Yee W Teh. Bayesian learning via stochastic gradient langevin dynamics. In *Proceedings of the 28th international conference on machine learning (ICML-11)*, pp. 681–688. Citeseer, 2011.

David H Wolpert and William G Macready. No free lunch theorems for optimization. *IEEE transactions on evolutionary computation*, 1(1):67–82, 1997.

Jaesik Yoon, Taesup Kim, Ousmane Dia, Sungwoong Kim, Yoshua Bengio, and Sungjin Ahn. Bayesian model-agnostic meta-learning. In *Proceedings of the 32nd International Conference on Neural Information Processing Systems*, pp. 7343–7353, 2018.

Sheheryar Zaidi, Arber Zela, Thomas Elsken, Chris Holmes, Frank Hutter, and Yee Whye Teh. Neural ensemble search for uncertainty estimation and dataset shift. *arXiv preprint arXiv:2006.08573*, 2020.

Hongpeng Zhou, Minghao Yang, Jun Wang, and Wei Pan. Bayesnas: A bayesian approach for neural architecture search. *CoRR*, abs/1905.04919, 2019.

Barret Zoph, Vijay Vasudevan, Jonathon Shlens, and Quoc V Le. Learning transferable architectures for scalable image recognition. In *Proceedings of the IEEE conference on computer vision and pattern recognition*, pp. 8697–8710, 2018.

A   PROOF OF COROLLARY 1.1

Proof. This can easily be seen by considering the result of Insight 1 for the last transformation in line 9.

$$\mathbb{E}_{x,D}[KL(p(\cdot|x,D),q_\theta(\cdot|x,D))] \tag{5}$$

$$= -\mathbb{E}_{x,D}\left[\int_y p(y|x,D)\log\frac{q_\theta(y|x,D)}{p(y|x,D)}\right] \tag{6}$$

$$= -\mathbb{E}_{x,D}\left[\int_y p(y|x,D)\log q_\theta(y|x,D)\right] + \mathbb{E}_{x,D}\left[\int_y p(y|x,D)\log p(y|x,D)\right] \tag{7}$$

$$= \mathbb{E}_{x,D}[\mathrm{H}(p(\cdot|x,D),q_\theta(\cdot|x,D))] - \mathbb{E}_{x,D}[\mathrm{H}(p(\cdot|x,D))]] \tag{8}$$

$$= \ell_\theta + C, \tag{9}$$

where $C = -\mathbb{E}_{x,D}[\mathrm{H}(\cdot|x,D)]$ is a constant that does not depend on θ.   □

B   PROOF OF COROLLARY 1.2

Proof. We assume a θ with $q_\theta = p$ exists and we know that the cross-entropy is minimized for equal distributions; thus the optimum θ^* fulfills $q_{\theta^*}(\cdot|x,D) = p(\cdot|x,D)$ for all x,D where the density of the prior fulfills $p(x,D) > 0$, which is exactly the subset for which the conditional is defined.   □

C   PROOF THEOREM 1

Proof. Given an arbitrary distribution p, an arbitrary bound ϵ. For arbitrary minimum (maximum) bucket borders a (b), we consider the function $b_\mathbf{B}$ that maps each position y to its bucket $b \in \mathbf{B}$, where $\mathbf{B}$ is an arbitrary set of buckets. We define the upper bound of p for each bucket

$$u(y) = \sup_{y'\in b_s(y)} p(y'). \tag{10}$$

Similarly, we define the lower bound

$$l(y) = \inf_{y'\in b_s(y)} p(y'). \tag{11}$$

For each of these we consider their log form, too. That is $\hat{u}(y) = \log u(y) = \sup_{y'\in b_s(y)}\log p(y')$ and $\hat{l}(y) = \log l(y) = \inf_{y'\in b_s(y)}\log p(y')$. We can move the log inside the sup (inf), since log is steadily increasing.

Integrals over $\hat{u}$ and $\hat{l}$ thus handily represent Darboux's upper and lower sums of $\log p$, if $\log p$ is Riemann integrable and finite. We assumed that p is Riemann integrable, thus $\log p$ is also integrable, since the composition of continuous functions, which $\log x$ is for $x > 0$, with an almost everywhere continuous function is almost everywhere continuous and any finite value x has a finite value $\log x$, if $x > 0$. The requirement $x > 0$ is given due to the assumed full support of p. Thus, we can use $\forall\epsilon'\exists\mathbf{B}. \int_a^b \hat{u}(y) - \hat{l}(y)dy < \epsilon'$. We define $t = \sup_{y\in[a,b]} p(y)$, $T = \sup_{y\in\mathbb{R}} p(y)$ and the total probability mass of the interval $P = p(y \in [a,b])$. We use $\epsilon' = \log 1/P$, which fulfills $\epsilon' > 0$ since p has full support and thus for any borders a and b we have $P < 1$, get $\mathbf{B}$ s.t.

$$\int_a^b \hat{u}(y) - \hat{l}(y)dy < \log\frac{1}{P} \tag{12}$$

$$\Rightarrow \int_a^b t(\hat{u}(y) - \hat{l}(y))dy < t\log 1/P \tag{13}$$

$$\Rightarrow \int_a^b t\log\frac{u(y)}{l(y)}dy < t\log 1/P \tag{14}$$

$$\Rightarrow \int_a^b u(y)\log\frac{u(y)}{l(y)}dy < t\log 1/P \tag{15}$$

Let c be a constant s.t. $cu(y)$ yields a valid probability distribution with $\int cu(y)dy = \int_a^b cu(y)dy = 1$.

$$\Rightarrow \int_a^b cu(y) \log \frac{u(y)}{l(y)} dy < ct \log 1/P \tag{16}$$

$$\Rightarrow \int_a^b cu(y) \log \frac{cu(y)}{l(y)} dy < ct \log 1/P + \int_a^b cu(y) \log c \tag{17}$$

$$\Rightarrow \int_a^b cu(y) \log \frac{cu(y)}{l(y)} dy < ct \log 1/P + \log c \tag{18}$$

We use $c < 1/P$, as $1/P$ would be the factor c' to make $\int_a^b c'p(y)dy = 1$ and c is this factor for $u(y)$, which has $u(y) \geq p(y)$ for any $y \in [a, b]$.

$$\Rightarrow \int_a^b cu(y) \log \frac{cu(y)}{l(y)} dy < ct \log 1/P + \log 1/P \tag{19}$$

$$\Rightarrow \int_a^b cu(y) \log \frac{cu(y)}{l(y)} dy < (ct + 1) \log 1/P \tag{20}$$

$$\Rightarrow \int_a^b cu(y) \log \frac{cu(y)}{l(y)} dy < -t \frac{\log P}{P} - \log P \tag{21}$$

$$\Rightarrow \int_a^b cu(y) \log \frac{cu(y)}{l(y)} dy < -T \frac{\log P}{P} - \log P \tag{22}$$

$$\Rightarrow \int_a^b cu(y) \log \frac{cu(y)}{p(y)} dy < -T \frac{\log P}{P} - \log P \tag{23}$$

$$\Rightarrow KL(cu(y), p(y)) < -T \frac{\log P}{P} - \log P \tag{24}$$

$$\Rightarrow KL(cu(y), p(y)) < -(T + P) \frac{\log P}{P} \tag{25}$$

$$\Rightarrow KL(cu(y), p(y)) < -(T + 1) \frac{\log P}{P}. \tag{26}$$

Here, $cu(y)$ is a valid bar distributions. Now we want to find a and b such that $-(T+1)\frac{\log P}{P} < \epsilon$, which is equivalent to

$$\frac{1}{P} \log 1/P < \frac{\epsilon}{T + 1} \tag{27}$$

Here, we can substitute the Lambert W function to arrive at the final result, that we should choose a and b such that $p([a, b]) \geq e^{-W_0(\frac{\epsilon}{T+1})}$, which is always possible as W_0 maps to $(0, \infty)$ for positive inputs, which we have with $\frac{\epsilon}{T+1}$. And we have that $e^{-x} < 1$ and $e^{-x} > 0$ for any $x \in (0, \infty)$.

Thus, we can conclude the proof. We could upper bound the *KL*-Divergence for any a and b. Then, based on that bound we found a setting for values a and b such that this upper bounds falls below ϵ.

$\square$

D   GENERAL TRANSFORMER TRAINING DETAILS

We follow the standard Transformer encoder setup. In the whole discussion one should note the crucial difference to a standard MLE training: Our optimization problem does not allow for overfitting. An improvement in training loss always means an improvement in the closeness to the exact posterior. More training just improves performance and calibration. The only exception of this is the fine-tuning done for the few-shot learning experiment in Section 7. We use Adam (Kingma & Ba, 2015) and cosine decay (Loshchilov & Hutter, 2016) with warmup. For all experiments we used a embedding size of 512, only for few-shot classification we used 1024. The only hyper-parameters that we did fine-tune for the Transformer training were the batch size and learning rate. Although, it usually was enough to choose a large enough batch size while the learning rate was more important. Learning

rates generally where chosen based on training performance, if not specified differently. We can do this as we generate new data during training and thus do not need to tune on held-out data. We saw that search over the set $\{.00001, .0001, .0003, .001\}$ for a learning rate generally yielded good enough results. Usually performance of the models got better with more training, thus the number of samples used for training generally depends on our compute budget. For setups models considered we could improve performance with more training. We stopped when we were satisfied with the results. We did not train longer than a few days on a single standard GPU for any PFN.
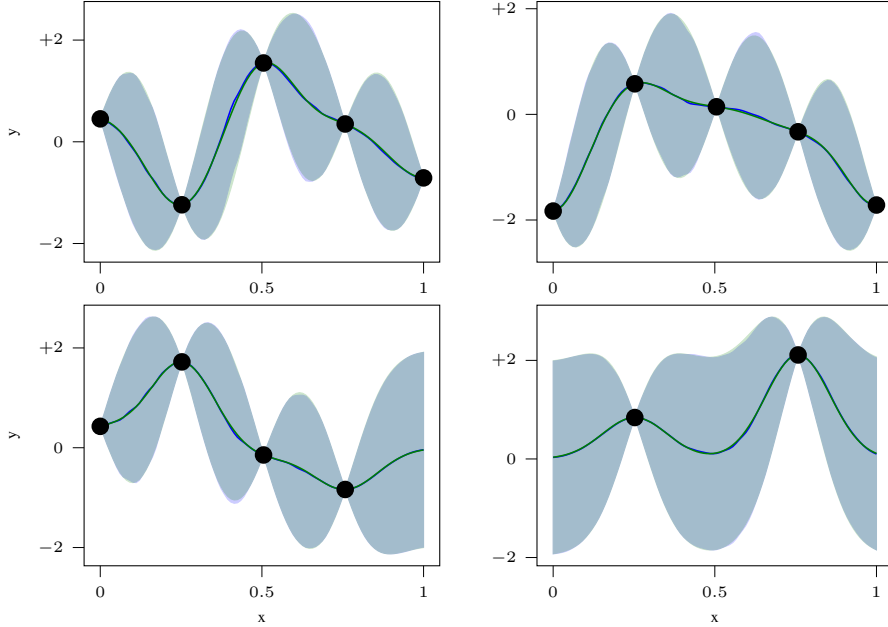

Figure 7: We show the mean and 95% intervals of the original GP posterior in green and the corresponding PFN approximations in blue. We used a length scale of 0.1.
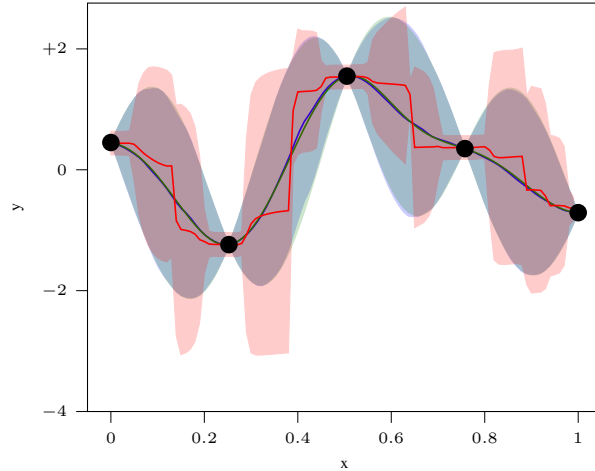
Figure 8: Like in plot 7, we show the mean and 95% confidence intervals for the exact GP prior in green and for our PFN in blue. (They are almost indistinguishable, with very small differences visible, e.g., at $x = 0.4$.) To further highlight what a big step forward our method is, we additionally show the respective values for the relatively new Attentive Neural Processes (ANP) (Kim et al., 2018). We trained both methods in very different environments, but ANP was clearly given the bigger budget.

17

E TRANSFORMER ADAPTIONS

E.1 AN EFFICIENT ARCHITECTURE

The first step of the model is to encode x and y; in all our experiments, we use simple linear layers for this, but one could also use other application-specific encoding layers. Our setup is equivariant to the ordering of the input dataset's examples. To achieve this, we remove positional encodings and feed (x, y) pairs together to the Transformer as a sum of their encodings; see Appendix E.3 for an ablation of the impact of the equivariance to the ordering. In practice, we feed query points together for efficiency reasons; these are the only inputs for which position matters, and we thus use the output at their positions as prediction for their corresponding PPD over y. Since different query points should not depend on each other, we use an attention mask that allows attention from every input example to every other input example and allows attention from every query points to every input example. An example of the model and its attention can be seen in Figure 2a.

During training, we fix the total number of inputs $N = n + m$, where n is the number of inputs and m is the number of queries, and sample n from a distribution, in order to allow the Transformer to learn to work with different dataset sizes. Since for smaller n we have more query points to train on, we over-sample larger n, s.t. the number of query points seen during training for each n is approximately equal. That is, we sample each $n \in \{0, \dots, N-1\}$ with a weight $1/m = 1/(N-n)$. As prediction head we use a softmax for multi-class classification tasks, a sigmoid for binary classification tasks and the Riemann distribution for regression.

E.2 RIEMANN DISTRIBUTION DEFINITION

Given a set of of buckets $\mathbf{B}$, where each bucket $b \in \mathbf{B}$ describes an interval such that

$$\bigcup_{b \in \mathbf{B}} b = [a, b] \tag{28}$$

and for any $b, b' \in \mathbf{B}$, we have $b \cap b' = \varnothing$. Additionally, we define the upper-bound (lower-bound) of the lowest (highest) bucket to be l (f), and a function $B(\cdot)$ that maps a $y \in \mathbb{R}$ to the unique bucket b with $y \in b$. We assume to have a function w mapping to the width of each bucket as $w(b) = \max_{y \in b} y - \min_{y \in b} y$. Lastly, we assume the model gives us a probability p_b for each bucket b.

In the finite case the Riemann distribution is defined as

$$p(y) = p_{b(y)}/w(b(y)). \tag{29}$$

We normalize with the width of the bucket since p_b describes the probability $p(y' \in b)$, but we are interested in the probability $p(y = y')$.

For the case of infinite support, we have

$$f(y_q) = \begin{cases} 2 \cdot f_{\mathcal{N}}(y_q - l), & \text{if } y_q \leq l \\ 2 \cdot f_{\mathcal{N}}(f - y_q), & \text{if } y_q \geq f \\ p_{b(y_q)}/b(y_q), & \text{otherwise.} \end{cases} \tag{30}$$

Here, the Half-Normal distributions are scaled such that half the probability weight is inside the bounds of the first (last) bucket.

E.3 ABLATION STUDIES

Above, we introduce a novel way of doing regression with neural networks that departs from the tradition of using normal distributions. Additionally, we remove the default positional embeddings from the Transformer. We show the impact of both approaches on the Transformer in Figure 9. Notice that, while the effect of the Riemann Distribution is very pronounced, the effect of making our architecture permutation invariant only slowly increases with sequence length. For each setup we searched over a set of the same four learning rates and evaluated the best performing on another sample from the distribution.
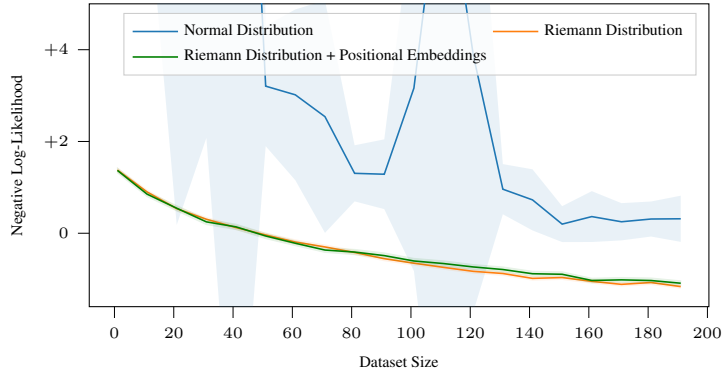
Figure 9: In this figure we show the impact of different architectural decisions on the performance of our method in fitting a Gaussian Process. We use the same Gaussian Process as in Section 5.1.

F   DETAILS FOR SECTION 5

The error intervals that can be seen in the Prior-Data NLL plots are 95% percent confidence intervals over different dataset samples from the prior.

Details for Section 5.1   Here, we generally followed default settings for GPs. That is, we used the RBF-Kernel with zero-mean, a length scale of 0.6, 1e-4 additional noise on the diagonal of the covariance matrix. The output scale was set to 1. Only for the plots in the Figure 7 and Figure 8 the length scale was decreased to 0.1. The experiments with more examples in Figure 4a did use 5 input dimension, while the qualitative visualizations only used one. For all methods we sample 1000 datasets for evaluation, each of which has a single validation example, for each dataset size.

Details for Section 5.2   In this section, we followed the default settings that can be found in BoTorch's *SingleTaskGP* (Balandat et al., 2020). We only changed the distribution over the diagonal noise, as the default is very high, such that it is hard to see any improvements with any of the methods in NLL with an increasing number of training samples. The GP is setup as a Matérn Kernel with $\nu = 2.5$ and we have the following hyper-priors: the noise was sampled from $\Gamma(\alpha = 0.0001, \beta = 1.0)$, the output scale from $\Gamma(\alpha = 2.0, \beta = 0.15)$ and the length scale from $\Gamma(\alpha = 3.0, \beta = 6.0)$.

We used the Pyro (Bingham et al., 2018) implementation of NUTS. Here, we used every sampled hyper-parameter setting as a sample GP. We averaged the output distribution over all sampled GPs to yield an approximation to the PPD. We scaled both the warmup and the rollout steps together: with "8 (warmup) steps" we mean 8 warmup steps and then 8 sampling steps.

Only the MCMC experiments were run on CPU, as this was faster than using the GPU. For all methods we sample 1000 datasets for evaluation, each of which has a single validation example, for each dataset size.

Details for Section 5.3   For SVI (Bayes-by-Backprop) we followed the setup of (Blundell et al., 2015) and used Adam (Kingma & Ba, 2015) as optimizer. We leveraged Pyro (Bingham et al., 2018) for optimization. We scaled both the training steps and number of samples averaged together to increase approximation quality.

For MCMC we used the Pyro (Bingham et al., 2018) implementation of NUTS and averaged the output distribution over all sampled BNNs to yield an approximation to the PPD. We scaled both the warmup and the rollout steps together to increase approximation performance. We used one MCMC chain. PFN and SVI are evaluated on a GPU (Nvidia Tesla V100) while MCMC is evaluated on a CPU since it was faster on CPU than on GPU.

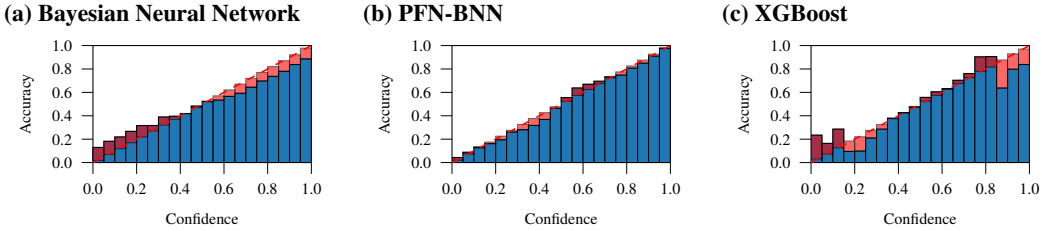**(a) Bayesian Neural Network**   **(b) PFN-BNN**   **(c) XGBoost**

Figure 10: Comparison of uncertainty calibration curves over all predictions on the evaluated datasets. The dotted line indicates perfect calibration.

G   DETAILS FOR SECTION 6

Accomodating a variable number of features Since the evaluated datasets used a variable number of features, the dimensionality of the input is variable. This can not be accommodated by the fixed size of the linear layer used in our PFNs. Thus, we fixed a maximum number of features (60) and extended the datasets to this maximum number by appending zeros. We did this during prior training, sampling the number of features uniformly at random alongside the model architecture and during inference. We rescale the features by a factor of $\frac{\text{max features}}{\text{features used}}$ during prior training and bayesian inference to keep the mean input scale constant with a varying feature number.

Degrees of freedom for model architectures The evaluated BNN models consider a wide range of model architectures, that is those architectures vary in terms of: number of layers, number of hidden units per layer, layer sparsity, standard deviation of Gaussian noise applied to each unit and activation function applied to each unit. This list can be easily extended by adapting the sampling procedure.

Tuning hyperparameter ranges for hyper-priors and cross-validation While the Transformer-based methods need no parameter tuning on each dataset individually, they still require setting the prior hyperparameters. This is similar to setting the range of hyperparameters in a cross-validation grid search and can be reused for all similar problems, e.g., all small-scale tabular classification. We therefore run a hyperparameter search on a second set of validation datasets, listed in Table 4. The hyperparameters considered in this grid search can be found in 5 In this search, we find good settings for all hyper-parameters of our priors for the average over all validation datasets. This search results in one final hyper-parameter setting and only one single Transformer model that is reused for all datasets. We use the same setup to find cross-validation ranges for our baselines.

Standardization of datasets Each subset is standardized to have zero mean and unit variance where the statistics for the standardization are only calculated on the samples considered by the model, thus without any dependence on the test set.

Runtimes of prior fitting step Fitting our transformer with GP prior was done over 100 epochs, taking 2:44h, while fitting the BNN prior took 3:14h for the same number of epochs. Crucially, this model is reused for all datasets.

H   DETAILS FOR SECTION 7

We searched for the hyper-parameters specified as inputs in Figure 11 with a grid search, where we measure performance on the training tasks as validation set. We then trained our model as a PFN on samples from this prior. After this stage we fine-tuned the model on the training tasks of Omniglot. Here, we applied translations and used a default batch size of 100. We used a learning rate of 1e-5 to yield the performance shown in the plot after sampling 500,000 samples from the training tasks. Unlike above, we sample over different samples of our fine-tuned model to yield the confidence interval, to follow the standard reporting on the Omniglot benchmark.

```
def pencil_stroke_prior(num_classes=2, size=28, min_max_strokes=(1,3),
        min_max_len=(5/28,20/28), min_max_start=(2/28,25/28),
        min_max_width=(1/28,4/28), max_offset=4/28, max_target_offset=2/28):
    classes = []
    for i in range(num_classes):
        num_strokes = random.randint(*min_max_strokes)
        len_strokes = [random.randint(int(size * min_max_len[0]),
                        int(size * min_max_len[1]))
                        for i in range(num_strokes)]
        stroke_start_points = [
            (random.randint(int(size * min_max_start[0]), int(size * min_max_start[1])),
            random.randint(int(size * min_max_start[0]), int(size * min_max_start[1])))
            for i in range(num_strokes)]
        stroke_directions = []
        # i = Image.fromarray(np.zeros((28,28), dtype=np.uint8))
        # draw = ImageDraw.Draw(i)
        for i in range(num_strokes):
            sp, length = stroke_start_points[i], len_strokes[i]
            counter = 0
            while True:
                if counter % 3 == 0:
                    length = random.randint(int(size * min_max_len[0]),
                        int(size * min_max_len[1]))
                    sp = (
                    random.randint(int(size * min_max_start[0]),
                        int(size * min_max_start[1])),
                    random.randint(int(size * min_max_start[0]),
                        int(size * min_max_start[1])))
                    stroke_start_points[i], len_strokes[i] = sp, length
                radians = random.random() * 2 * math.pi
                x_vel = math.cos(radians) * length
                y_vel = math.sin(radians) * length
                new_p = (sp[0] + x_vel, sp[1] + y_vel)
                if not any(n > size - 1 or n < 0 for n in new_p):
                    break
                counter += 1
            stroke_directions.append(radians)
        classes.append((len_strokes, stroke_start_points, stroke_directions))
    generator_functions = []
    for c in classes:
        def g(c=c):
            len_strokes, stroke_start_points, stroke_directions = c
            i = Image.fromarray(np.zeros((size, size), dtype=np.uint8))
            draw = ImageDraw.Draw(i)
            width = random.randint(int(size * min_max_width[0]),
                            int(size * min_max_width[1]))
            offset = (random.randint(int(-size * max_offset), int(size * max_offset)),
                    random.randint(int(- size * max_offset), int(size * max_offset)))
            for sp, length, radians in \textbackslash
                    zip(stroke_start_points, len_strokes, stroke_directions):
                sp = (sp[0] + offset[0], sp[1] + offset[1])
                x_vel = math.cos(radians) * length
                x_vel += random.randint(int(-size * max_target_offset),
                                int(size * max_target_offset))
                y_vel = math.sin(radians) * length
                y_vel += random.randint(int(-size * max_target_offset),
                                int(size * max_target_offset))
                new_p = (sp[0] + x_vel, sp[1] + y_vel)
                stroke_directions.append(radians)
                draw.line([round(x) for x in sp + new_p], fill=128, width=width)
            a_i = np.array(i)
            a_i[a_i == 128] = np.random.randint(200, 255, size=a_i.shape)[a_i == 128]
            return Image.fromarray(a_i).filter(ImageFilter.GaussianBlur(.2))
        generator_functions.append(g)
    return generator_functions
```

Figure 11: A prior definition for a prior over straight strokes in python.

Name	Number of Features	Number of Symbolic Features
kr-vs-kp	37	37
credit-g	21	14
vehicle	19	1
wine	14	1
kc1	22	1
airlines	8	5
bank-marketing	17	10
blood-transfusion-service-center	5	1
phoneme	6	1
covertype	55	45
numerai28.6	22	1
connect-4	43	43
car	7	7
Australian	15	9
segment	20	1
jungle_chess_2pcs_raw_endgame_complete	7	1
sylvine	21	1
MiniBooNE	51	1
jannis	55	1
helena	28	1

Table 3: Tabular datasets used for evaluation. Taken from the OpenML AutoML Benchmark (filtered for $N_{features} \leq 100$, no missing values.)

Name	Number of Features	Number of Symbolic Features
haberman	4	2
ionosphere	35	1
sa-heart	10	2
cleve	14	9
four	2	0
german	24	0

Table 4: Tabular datasets used to find good general hyperparameters for hyper-priors as well as hyperparameters used in baseline cross-validation.

Figure 12: In this figure we show different samples from our prior for Omniglot data.

index	n	param
prior_activations	1	torch.nn.Tanh
	2	torch.nn.ReLU
prior_dropout_sampler	1	lambda: 0.0
	2	lambda: 0.5
	3	beta_sampler_f(1.1, 1.4)
	4	beta_sampler_f(1.1, 2.0)
	5	beta_sampler_f(1.1, 4.0)
	6	beta_sampler_f(2.0, 1.4)
	7	beta_sampler_f(2.0, 4.0)
prior_emsize_sampler	1	scaled_beta_sampler_f(1.1, 1.3, 256, max_features)
	2	scaled_beta_sampler_f(1.1, 2.0, 256, max_features)
	3	scaled_beta_sampler_f(1.1, 4.0, 256, max_features)
	4	scaled_beta_sampler_f(2.0, 4.0, 100, 1+max_features)
prior_nlayers_sampler	1	lambda: 3
	2	scaled_beta_sampler_f(1.1, 1.3, 4, 3)
	3	scaled_beta_sampler_f(1.1, 2.0, 5, 2)
	4	scaled_beta_sampler_f(1.1, 4.0, 5, 2)
	5	scaled_beta_sampler_f(2.0, 4.0, 4, 3)
prior_noise_std_gamma_k	1	range: [1.5, 5.0]
prior_noise_std_gamma_theta	1	range: [0.01, 1.0]
prior_sigma_gamma_k	1	range: [1.5, 5.0]
prior_sigma_gamma_theta	1	range: [0.01, 1.0]

Table 5: Hyperparameters considered during grid search tuning of the PFN-BNN on validation datasets. The activation functions refer to the activation function used in the data generating BNN and not the ones used in the PFN transformer. scaled_beta_sampler_f(a,b,max,min) refers to sampling from a beta distribution with parameters a, b (numpy.random.beta), scaling the output range from [0, 1] to [max, min] and then rounding the output to the integer range. beta_sampler_f(a, b) refers to a function that samples from the beta distribution without scaling and rounding.

Log. Regr.	{'solver': ['saga'], 'penalty': ['l1', 'l2', 'none'], 'tol': [0.01, 0.0001, 1e-10], 'max_iter': [500], 'fit_intercept': [True, False], 'C': [1e-05, 0.001, 0.01, 0.1, 1.0, 2.0]}
KNN	{'n_neighbors (max number of samples)': array([1, 2, 3, 4, 5])}
BNN	{'embed': [5, 10, 30, 64], 'lr': [0.001, 0.0001], 'num_training_steps': [400], 'num_samples_for_prediction': [400]}
GP	{'params_y_scale': [0.05, 0.1, 0.5, 1.0, 5.0, 10.0], 'params_length_scale': [0.1, 0.5, 1.0, 2.0]}
Catboost	{'learning_rate': [0.1, 0.5, 1.0], 'depth': [2, 4, 7], 'l2_leaf_reg': [0.0, 0.5, 1], 'iterations': [10, 40, 70], 'loss_function': ['Logloss']}
XGB	{'min_child_weight': [0.5, 1.0], 'learning_rate': [0.02, 0.2], 'subsample': [0.5, 0.8], 'max_depth': [1, 2], 'colsample_bytree': [0.8], 'eval_metric': ['logloss'], 'n_estimators': [100]}

Table 6: Hyperparameters used in cross-validation for each baseline method.

	PFN-BNN	PFN-GP	logistic	GP	KNN	BNN	Catboost	XGB
kr-vs-kp	0.928	0.897	0.920	0.886	0.754	0.843	0.653	**1.000**
credit-g	0.671	**0.681**	0.621	0.562	0.593	0.607	0.602	0.637
vehicle	0.562	0.501	**0.601**	0.506	0.527	0.562	0.525	0.522
wine	0.959	**0.975**	0.944	0.785	0.900	0.919	0.908	0.930
kc1	0.614	0.695	0.730	0.695	0.666	0.724	0.708	**0.747**
airlines	0.916	0.896	0.913	0.873	0.834	0.907	0.982	**0.985**
bank-market..	0.878	0.877	0.811	0.857	0.810	0.849	**0.908**	0.885
blood-transfus..	**0.588**	0.576	0.558	0.577	**0.588**	0.555	0.565	0.531
phoneme	0.757	0.782	0.735	**0.785**	0.772	0.733	0.766	**0.785**
covertype	**0.962**	0.904	0.904	0.929	0.793	0.870	0.810	0.798
numerai28.6	0.449	0.454	0.460	**0.502**	**0.502**	0.454	**0.502**	0.464
connect-4	**0.981**	0.961	0.951	0.933	0.871	0.934	0.945	0.976
car	**0.959**	0.926	0.925	0.771	0.874	0.935	0.849	0.898
Australian	**0.906**	0.903	0.862	0.866	0.865	0.873	0.848	0.871
segment	**1.000**	**1.000**	**1.000**	0.999	0.985	0.999	**1.000**	**1.000**
jungle_chess..	0.774	0.780	0.693	**0.852**	0.747	0.708	0.841	0.708
sylvine	0.833	0.791	0.915	0.708	0.664	0.785	0.885	**0.929**
MiniBooNE	0.855	0.852	0.821	0.843	0.850	**0.861**	0.818	0.855
dionis	**0.996**	0.977	0.981	0.982	0.962	0.987	0.975	0.991
jannis	**0.654**	0.652	0.570	0.551	0.569	0.549	0.603	0.600
helena	**0.911**	0.892	0.839	0.870	0.842	0.882	0.870	0.905
Mean rank AUC	**2.786**	3.833	4.690	5.286	6.214	5.000	4.833	3.357
Win/Tie/Loss AUC vs T-BNN	0/21/0	14/1/6	16/1/4	17/0/4	17/1/3	17/1/3	13/1/7	12/2/7
Wilcoxon p. AUC vs T-BNN	0.0e+00	3.6e-13	3.6e-13	3.9e-13	3.6e-13	3.6e-13	1.9e-12	1.6e-06
Benchmark Time	GPU: 0:00:13 CPU: 0:04:23		0:09:56	0:24:30	0:00:34	12:04:41	2:05:20	20:59:46
ECE	**0.025**	0.067	0.157	0.095	0.093	0.089	0.157	0.066

Table 7: ROC AUC Comparison: Evaluation is made on subsets of datasets with 30 training samples. 20 data-subsets are evaluated for each dataset. The ECE is a calibration measure. The novel PFN-BNN performs strongest overall.